Copyright 2016, California Institute of Technology. Govt. Sponsorship Acknowledged.

Silicon Micromachined Modulated Metasurface Antennas in the Terahertz Range

David González-Ovejero[1], Theodore J. Reck[1], Cécile D. Jung-Kubiak[1], Maria Alonso-DelPino[1], Goutam Chattopadhyay[1]
[1]Jet Propulsion Laboratory, California Institute of Technology, Pasadena, CA 91109, United States
{david.gonzalez, theodore.reck, cecile.d.jung, maria.alonso, goutam.chattopadhyay}@jpl.nasa.gov

***Abstract*—This paper explores the capabilities of a class of metasurface (MTS), which consists of metalized cylinders on a ground plane, for the realization of modulated MTS antennas at terahertz (THz) frequencies. The proposed structure is particularly appropriate for being micromachined out of a silicon wafer by means of deep reactive ion etching (DRIE). The constraints that DRIE imposes in the design of the MTS unit cell are discussed, along with the advantages of silicon micromachined modulated MTSs with respect to other fabrication approaches in the THz range.**

***Index Terms*—deep-reactive ion etching, leaky-waves, metasurfaces, silicon micromachining, terahertz frequencies.**

I. Introduction

Modulated metasurface (MTS) [1], [2] antennas have recently sprung up as a versatile solution for deep space communications [2]. Indeed, modulated MTSs can be applied to the design of high to very-high gain antennas. Among their advantages it is worth noting their capability of beam shaping, pointing and scanning, a simple on-surface control of the aperture fields, and all this while keeping a low profile and low envelope. The latter two features are particularly appealing for spaceborne communication systems and science instruments.

In MTS antennas, an inductive surface reactance supports the propagation of a (dominantly) transverse magnetic (TM) surface-wave (SW), which is gradually radiated. Radiation is achieved by periodically modulating the equivalent reactance on the antenna aperture. The interaction between the SW and the periodic modulation makes the (-1) indexed Floquet mode enter the visible region, thus becoming a radiating mode. The surface reactance modulation is typically achieved at microwave frequencies by changing the size and orientation of sub-wavelength patches printed on a grounded dielectric substrate, and arranged in a periodic lattice [1], [2]. MTSs made of printed patches are normally excited by a coaxial cable with capacitive loading for an improved matching.

Despite the good performance shown by artificial surfaces implemented with sub-wavelength patches at frequencies below 100 GHz, there are some aspects which hinder the use of this approach in the terahertz (THz) range. First, the losses in the dielectric become, in most applications, a limiting factor and all-metal structures are preferred. Second, it is challenging to combine a coaxial SW launcher with the rectangular waveguide (RW) output of solid-state frequency-multiplied continuous-wave sources, which are the most commonly used sources at THz frequencies [3]. The conversion of the RW transverse electric (TE) TE_{10} mode to the coaxial transverse electromagnetic (TEM) mode requires a long coaxial section, which implies large diameter/height ratios of the coaxial inner conductor. Hence, such feeding topologies will be mechanically unstable without any dielectric support and all-waveguide solutions are pursued.

Silicon micromachined components have been recently shown to provide an excellent performance in the sub-millimeter wave range [4]. Among the existing techniques, deep reactive ion etching (DRIE) is particularly well-adapted for micromachining integrated front-ends. Since it is based on etching, one may argue that it is challenging to maintain straight sidewalls and uniform depth across the wafer for each depth step. Nevertheless, these drawbacks can be overcome by extensive process development [5] and a thorough design. After carrying out the desired number of etching steps, $2\,\mu$m of gold is deposited by sputtering to metallize the structure.

In this paper we will demonstrate the suitability of silicon micromachining for the realization of modulated MTS antennas at millimeter and sub-millimeter wavelengths. The advantages of silicon micromachined modulated MTSs with respect to other fabrication approaches in the THz range will be also discussed.

II. Sinusoidally modulated reactance surfaces

As mentioned in the Introduction, one can transform a SW into a leaky-wave (LW) by appropriately modulating a surface reactance. Let us first consider a one-dimensional modulation on the $z = 0$ plane and no variation in the y direction. The corresponding sinusoidal inductive reactance can be written as

$$\mathrm{X_s}\left(x\right) = \bar{\mathrm{X}}\left(1 + M\sin\left(\frac{2\pi}{d}\,x\right)\right) \tag{1}$$

where $\bar{\mathrm{X}}$ is the average surface reactance, M is the modulation factor and d is the period of the modulation. This case was studied by Oliner and Hessel in [6]. The solution to the periodic problem consists in an infinite series of Floquet modes, the transverse-to-z wavenumber for the n-indexed mode is

$$k_{t,n} = \beta_{\mathrm{sw}} + \beta_{\Delta} - \mathrm{j}\alpha + \frac{2\pi n}{d} \tag{2}$$

where β_{Δ} and α are perturbations in the phase and attenuation constants, respectively, which depend on $\bar{\mathrm{X}}$, M and d. In turn,

$\beta_{\rm sw}$ stands for the unperturbed value of k_t ($M=0$), obtained by imposing the transverse resonance condition between $\mathrm{j}\bar{\mathrm{X}}$ and the free-space TM impedance

$$\mathrm{j}\bar{\mathrm{X}} + Z_{0,\mathrm{TM}} = 0 \tag{3}$$

Since we are looking for SWs $\beta_{\rm sw} > k$ and $Z_{0,\mathrm{TM}} = -\mathrm{j}\zeta\sqrt{\beta_{\rm sw}^2 - k^2}/k$, with k and ζ being the free-space wavenumber and impedance, respectively. Solving for $\beta_{\rm sw}$ in (3) gives $\beta_{\rm sw} = k\sqrt{1+(\bar{\mathrm{X}}/\zeta)^2}$.

When $|\Re\{k_{t,n}\}| < k$, the corresponding mode enters in the visible region of the spectrum, and it can be identified as a LW solution. The $n=-1$ mode is the dominant leaky-mode, and it radiates in a direction given by

$$\beta_{\rm sw} + \beta_\Delta - 2\pi/d = k\sin\theta_0 \tag{4}$$

where θ_0 is the angle with respect to the z axis. Consequently, for a single beam directed at an angle θ_0, $\bar{\mathrm{X}}$ and d can be related using $\beta_{\rm sw} = k\sqrt{1+(\bar{\mathrm{X}}/\zeta)^2}$ in (4). For instance, one can generate a single forward beam using a period d

$$d/\lambda = 1/\left(\sqrt{1+(\bar{\mathrm{X}}/\zeta)^2} - \sin\theta_0\right) \tag{5}$$

when $\bar{\mathrm{X}}/\zeta > \sqrt{4\sin\theta_0(1+\sin\theta_0)}$. In the derivation of (5), the effect of β_Δ ($<< \beta_{\rm sw}$) has been neglected.

III. Constituent elements for THz MTSs

The proposed MTS consists in a periodic array of metallic cylinders arranged in a square lattice, and placed on a ground plane. Such structure, which resembles a Fakir's bed of nails, has been used in the past for synthesizing artificial surfaces of inductive nature [7]. Starting from the reflection coefficient for an impinging TM wave derived in [8, eq. 4] for a bed of nails of uniform height, one can write the equivalent MTS surface reactance as

$$\mathrm{X} = \zeta\,(1-\xi)\tan(kh) - \xi\,\alpha_{\rm TM}\,\tanh(\alpha_{\rm TM}h) \tag{6}$$

where h is the height of the cylindrical pins, $\xi = \beta_{\rm sw}^2/(\beta_{\rm p}^2 + \beta_{\rm sw}^2)$, and $\alpha_{\rm TM} = \sqrt{\beta_{\rm p}^2 + \beta_{\rm sw}^2 - k^2}$. The parameter ξ accounts for the power coupled to the TEM mode in the bed of nails, which can be also excited by the incoming TM wave. On the other hand, $\alpha_{\rm TM}$ is the propagation (attenuation) constant [8] of the TM mode in the wired medium. Finally, $\beta_{\rm p}$ is the "plasma wavenumber" [8, eq. 2]

$$\beta_{\rm p} = \frac{1}{a}\sqrt{\frac{2\pi}{\ln\left(\frac{a}{2\pi r}\right) + 0.5275}} \tag{7}$$

where r is the radius of the cylinder and a the side of the square lattice. The parameter $\beta_{\rm p}$ accounts for the spatial dispersion in the wired medium.

The expression in (6) represents the bed of nails as a continuous medium, and it is valid when the aspect ratio $h/a >> 1$ [8]. The parameter a in a modulated MTS is given by $a = d/N$, where N is the number of unit cells used to represent one period, and it depends on $\bar{\mathrm{X}}$ and θ_0. One could try to make h arbitrarily long to satisfy $h/a >> 1$.

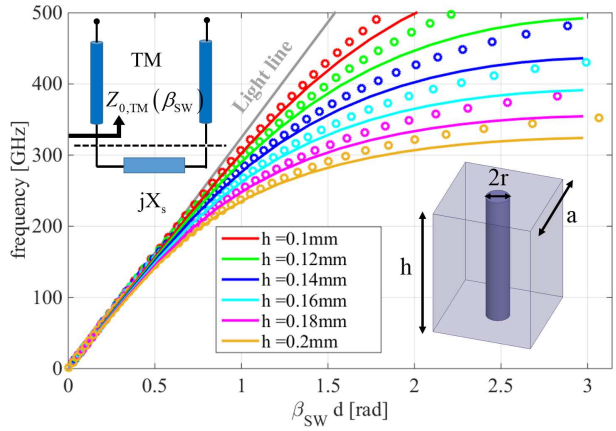

Fig. 1. Dispersion diagrams for different heights of the metallic cylinders, $r = 17.5\,\mu$m and the side of the square unit cell is $a = 147\,\mu$m. The solid lines have been obtained using the eigenmode solver in [9]. The circular markers are the solution of (3) for the reactance given in (6).

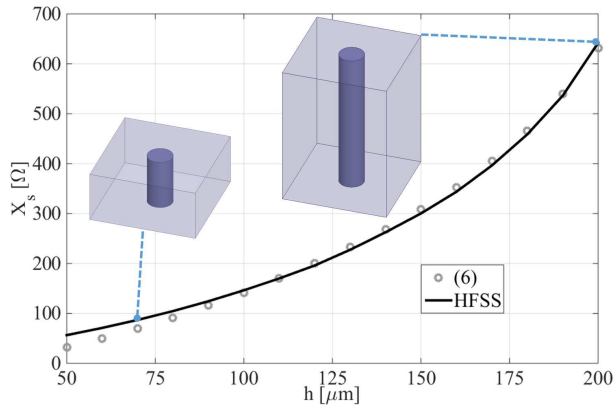

Fig. 2. Surface reactance at 300GHz as a function of the height of the cylinder. The cylinder radius is $r = 17.5\,\mu$m and the side of the unit cell is $a = 147\,\mu$m. The solid line represents the values obtained solving (3) for the frequency-$\beta_{\rm sw}$ pairs obtained with a full-wave eigenmode solver [9]. The circular markers have been obtained using (6).

Unfortunately, long cylindrical rods are difficult to realize with DRIE while keeping a good precision and a simple process. Therefore, upon choosing $\bar{X}$ and N, one has to verify that the required heights satisfy $h/r \leq 10$ before proceeding with the design.

Fig. 1 shows the dispersion curves corresponding to metallic cylinders of different heights, with $r = 17.5\,\mu$m and fixed side a of the square lattice. The period d has been computed at 300 GHz using (5) for an average impedance $\bar{\mathrm{X}} = 0.7\zeta$, a forward beam pointing at $\theta_0 = 5^o$ and $N = 6$, which implies $a = 147\,\mu$m. The solid curves in Fig. 1 have been obtained with the eigenmode solver of a commercial software [9], whereas the points have been computed imposing (3) between X in (6) and the TM free-space impedance (see equivalent circuit in the inset). Since $h/a \leq 1.4$, the agreement between the analytical approximation and the full-wave solution is not very good. Nevertheless, if one compares the retrieved surface reactances (shown in Fig. 2), the analytical approximation is still valid for a significant range of heights h. Therefore, the homogenization approach has to be used with caution when designing this type

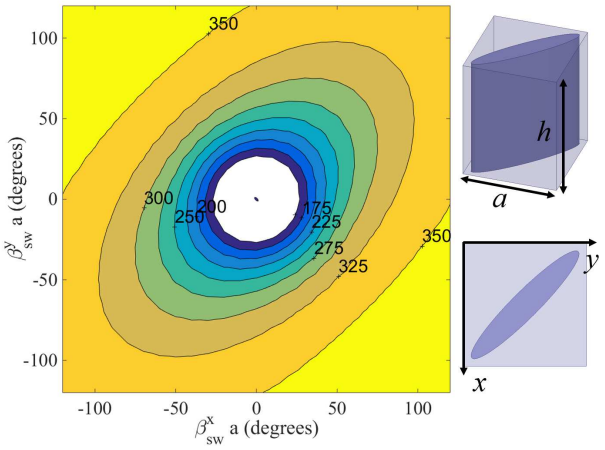

Fig. 3. Isofrequency dispersion contours for the unit cell depicted in the insets. The unit cell's side is $a = 138.5\,\mu$m, the height of the cylinder is $h = 180\,\mu$m, and the elliptical cross-section has minor axis equal to $30\,\mu$m and axial ratio equal to 4.

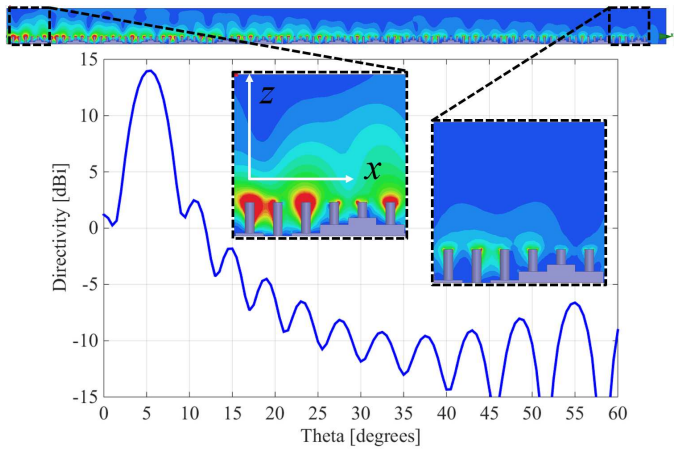

Fig. 4. Directivity pattern for a row of cylinders modulated according to (1) with $\bar{\mathrm{X}} = 0.7\zeta$ and $M = 0.6$. The insets show the E-field intensity in the $y = 0$ plane and the attenuation of the SW due to radiation.

of modulated MTS antennas.

A major advantage of DRIE is that one can choose to etch complex cross-sections. This feature can be exploited to synthesize anisotropic surface reactances, which provide additional degrees of freedom for controlling the aperture fields' polarization [1, Sec. IV] [2, Sec. V]. Other novel approaches to the design of modulated MTS antennas in the THz range, like graphene [10], do not offer this capability and micromachined textured surfaces have an edge in this respect.

In general, the surface reactance is a tensor, which depends on the transverse wave vector $\underline{\beta}_{\mathrm{sw}} = \beta^x_{\mathrm{sw}}\,\hat{x} + \beta^y_{\mathrm{sw}}\,\hat{y}$ and relates the transverse electric and magnetic fields (evaluated at the upper interface) as

$$\vec{E}_t|_{z=0^+} = \mathrm{j}\underline{\underline{\mathrm{X}}}_{\mathrm{S}} \cdot \hat{\mathrm{z}} \times \vec{H}_t|_{z=0^+} \tag{8}$$

where $\underline{\underline{\mathrm{X}}}_{\mathrm{S}} = [[\mathrm{X}_{xx}\,\mathrm{X}_{yx}]^{\mathrm{T}}\,[\mathrm{X}_{xy}\,\mathrm{X}_{yy}]^{\mathrm{T}}]$ is defined in Cartesian coordinates, and $\hat{\mathrm{z}}$ is the normal to the MTS plane. Nevertheless, for an electrically small constant period, the surface reactance of a unit cell with rotational symmetry order higher than two (circular or square cross-sections) is scalar (1). This is not the case for cylinders of elliptical cross section, which will provide a different response when the SW wave vector is aligned with each of the two symmetry axes of the ellipse. Fig. 3 shows the isofrequency dispersion ellipses for an elliptical cylinder with minor axis equal to $30\,\mu$m and axial ratio equal to 4, in a square unit cell with side $a = 138.5\,\mu$m. The unit cell possesses two orthogonal symmetry axes, which principal directions can be identified, in the low frequency regime, with the principal axes of the dispersion ellipse. The surface reactance tensor at a given frequency can be retrieved from the corresponding isofrequency dispersion ellipse by fitting, in the least square sense, the simulated data with [11, eq. 19]

$$\begin{aligned}&(1 + \mathrm{X}_{xx}\mathrm{X}_{yy} - \mathrm{X}_{xy}\mathrm{X}_{yx})\,k\,k_z + (\mathrm{X}_{xy} + \mathrm{X}_{yx})\,\beta^x_{\mathrm{sw}}\,\beta^y_{\mathrm{sw}} \\ &+ \left[(\mathrm{X}_{xx} + \mathrm{X}_{yy})\,k^2 - \mathrm{X}_{xx}(\beta^y_{\mathrm{sw}})^2 - \mathrm{X}_{yy}(\beta^x_{\mathrm{sw}})^2\right] = 0\end{aligned} \tag{9}$$

where $k_z = \sqrt{(\beta^x_{\mathrm{sw}})^2 + (\beta^y_{\mathrm{sw}})^2 - k^2}$. For instance, the case pictured in Fig. 3 represents an artificial tensor surface with $\underline{\underline{\mathrm{X}}}_{\mathrm{S}} = \zeta[[1.04\,,\,0.46]^{\mathrm{T}}\,[0.46\,,\,1.03]^{\mathrm{T}}]$.

By changing the height, orientation and axial ratio of the elliptical cylinders, each component of the tensor will undergo a different modulation. This feature can be exploited to drastically reduce the level of the cross-polarized far-field components [2, Sec. 2] [12]. The design strategy for anisotropic beds of nails will be discussed in the conference and it is omitted here not to render the paper unnecessarily long.

IV. Design Examples

The first example presents a verification of the theory in Sec. II and Sec. III. The simulation consists in a row of cylindrical rods oriented along x. The surface reactance has been modulated according to (1) with $\bar{\mathrm{X}} = 0.7\zeta$ and $M = 0.6$, and the design frequency is 300 GHz. The value of d at this frequency for the modulation above and a pointing angle $\theta_0 = 5^o$ is $d = 882\,\mu$m. For $N = 6$, one has $a = d/N = 147\,\mu$m. The total length of the row is $15d$. Full-wave results from an eigenmode solver (see Fig. 2) or (6) can be used to obtain the height of the cylinder that one needs to realize the surface reactance at each unit cell. The structure is excited by a wave port with vertical electric field, and the row of cylinders is sandwiched by two perfect magnetic planes to maintain a field distribution that supports the TM SW. Fig. 4 shows the directivity pattern of the structure obtained with HFSS [9], this results confirms the presence of a beam pointing in the desired direction. On the other hand, one can see in the insets the effect of the SW attenuation as it gets radiated along the structure.

The second example consists in a spiral modulated MTS antenna. The spiral has been designed at 300 GHz and it provides a broadside pencil beam with circular polarization. The synthesized surface reactance is

$$X_s\,(x) = \bar{\mathrm{X}}\left(1 + M\sin\left(\frac{2\pi}{d}\,\rho - \phi\right)\right) \tag{10}$$

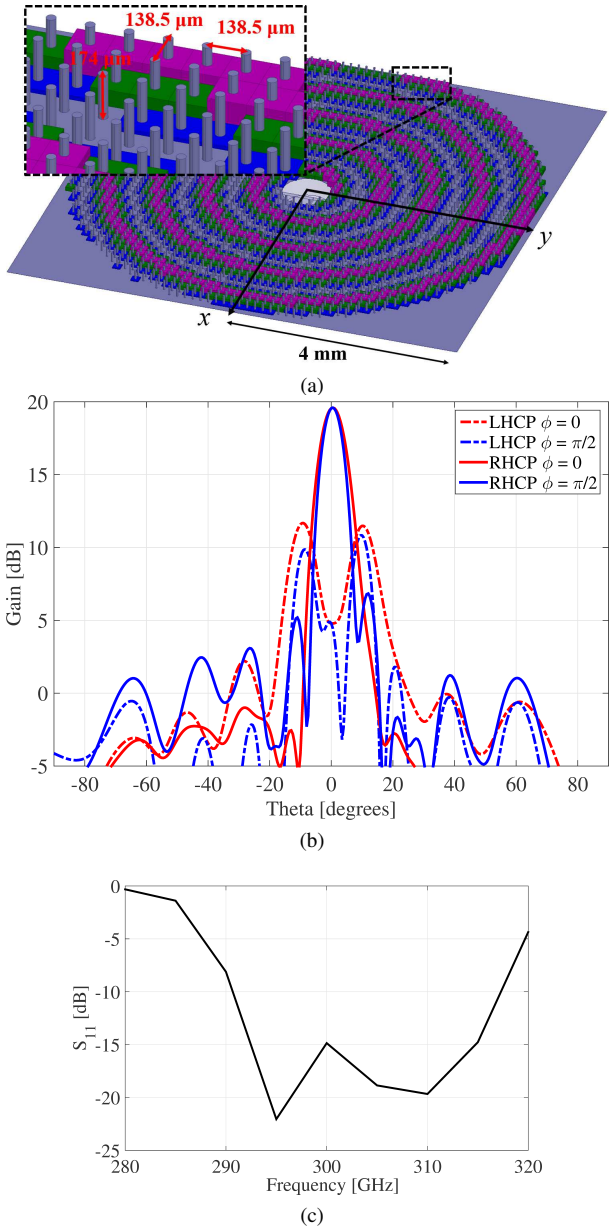

Fig. 5. (a) Simulated spiral modulated MTS antenna, (b) Right-handed circular polarized (RHCP) and left-handed circular polarized (LHCP) gain patterns at 300 GHz plotted with solid and dashed lines, respectively, on two orthogonal cuts. (c) S_{11} at the input RW port of the antenna.

where ρ and ϕ represent the position on the MTS plane in polar coordinates. The reader is referred to [2, Sec. IV-A] for further details. In our case, $\bar{X} = 0.7\zeta$, $M = 0.65$, $N = 6$ and $a = 138.5\,\mu$m. The structure is shown in Fig. 5a, where each color represents a different height of the metallic cylinders. The far-field gain patterns have been computed with HFSS [9] and they are shown in Fig. 5b for two orthogonal planes. The structure is fed with a overmoded circular waveguide with only the TM_{01} mode propagating, this mode provides an efficient excitation of the TM surface wave on the MTS plane, while avoiding the use of a coaxial feed. The feeder (not shown here) is placed underneath the MTS and it transforms the TE_{10} mode in the input RW to the TM_{01} in the CW. The S_{11} obtained with the aforementioned feeding structure is shown in Fig. 5c.

V. Conclusion

A bed of nails MTS made of cylinders with circular or elliptical cross-section is proposed for the design of modulated MTS antennas in the THz range. This structure is particularly well-suited for being micromachined out of a silicon wafer by means of deep reactive ion etching (DRIE). The constraints that DRIE imposes on the design are discussed, along with the advantages of silicon micromachined modulated MTSs with respect to other fabrication approaches in the THz range. An aspect of major interest is the possibility of realizing anisotropic impedance boundary conditions with all-metallic structures at THz frequencies.

Acknowledgment

This work has been carried out at the Jet Propulsion Laboratory, California Institute of Technology, under a contract with National Aeronautics and Space Administration (NASA).

The work of D. González-Ovejero was supported by a Marie Curie International Outgoing Fellowship within the 7th European Community Framework Programme.

References

[1] B. Fong, J. Colburn, J. Ottusch, J. Visher, and D. Sievenpiper, "Scalar and tensor holographic artificial impedance surfaces," *IEEE Trans. Antennas Propag.*, vol. 58, no. 10, pp. 3212–3221, Oct. 2010.

[2] G. Minatti, M. Faenzi, E. Martini, F. Caminita, P. De Vita, D. González-Ovejero, M. Sabbadini, and S. Maci, "Modulated metasurface antennas for space: Synthesis, analysis and realizations," *IEEE Trans. Antennas Propag.*, vol. 63, no. 4, pp. 1288–1300, Apr. 2015.

[3] G. Chattopadhyay, "Technology, capabilities, and performance of low power terahertz sources," *IEEE Trans. THz Sci. Technol.*, vol. 1, no. 1, pp. 33–53, Sep. 2011.

[4] T. Reck, C. Jung-Kubiak, J. Gill, and G. Chattopadhyay, "Measurement of silicon micromachined waveguide components at 500–750 GHz," *IEEE Trans. THz Sci. Technol.*, vol. 4, no. 1, pp. 33–38, Jan. 2014.

[5] C. Jung, B. Thomas, C. Lee, A. Peralta, J. Gill, K. Cooper, G. Chattopadhyay, E. Schlecht, R. Lin, and I. Mehdi, "Compact submillimeter-wave receivers made with semiconductor nano-fabrication technologies," in *Proc. IEEE Int. Microw. Symp. (IMS)*, Jun. 2011, pp. 1–4.

[6] A. Oliner and A. Hessel, "Guided waves on sinusoidally-modulated reactance surfaces," *IRE Trans. Antennas Propag.*, vol. 7, no. 5, pp. 201–208, Dec. 1959.

[7] R. King, D. V. Thiel, and K. Park, "The synthesis of surface reactance using an artificial dielectric," *IEEE Trans. Antennas Propag.*, vol. 31, no. 3, pp. 471–476, May 1983.

[8] M. Silveirinha, C. Fernandes, and J. Costa, "Electromagnetic characterization of textured surfaces formed by metallic pins," *IEEE Trans. Antennas Propag.*, vol. 56, no. 2, pp. 405–415, Feb. 2008.

[9] ANSYS Inc., "HFSS, Version 15," Pittsburgh, PA, 2015.

[10] M. Esquius-Morote, J. Gomez-Diaz, and J. Perruisseau-Carrier, "Sinusoidally modulated graphene leaky-wave antenna for electronic beam-scanning at thz," *IEEE Trans. THz Sci. Technol.*, vol. 4, no. 1, pp. 116–122, Jan. 2014.

[11] H. Bilow, "Guided waves on a planar tensor impedance surface," *IEEE Trans. Antennas Propag.*, vol. 51, no. 10, pp. 2788–2792, Oct. 2003.

[12] D. González-Ovejero and S. Maci, "Gaussian ring basis functions for the analysis of modulated metasurface antennas," *IEEE Trans. Antennas Propag.*, vol. 63, no. 9, pp. 3982–3993, Sep. 2015.

©2015 California Institute of Technology.
Government sponsorship acknowledged.